Article:

Konrad, H, Shepherd, A, Gilbert, L et al. (4 more authors) (2018) Net retreat of Antarctic glacier grounding lines. Nature Geoscience, 11. pp. 258-262. ISSN 1752-0894

https://doi.org/10.1038/s41561-018-0082-z

Net retreat of Antarctic glacier grounding lines

Hannes Konrad[1,2], Andrew Shepherd[1], Lin Gilbert[3], Anna E. Hogg[1], Malcolm McMillan[1], Alan Muir[3], Thomas Slater[1]

Affilitations

[1]Centre for Polar Observation and Modelling, University of Leeds, United Kingdom

[2]Alfred Wegener Institute, Helmholtz Centre for Polar and Marine Research, Bremerhaven, Germany

[3]Centre for Polar Observation and Modelling, University College London, United Kingdom

Grounding lines are a key indicator of ice-sheet instability, because changes in their position reflect imbalance with the surrounding ocean and impact on the flow of inland ice. Although the grounding lines of several Antarctic glaciers have retreated rapidly due to ocean-driven melting, records are too scarce to assess the scale of the imbalance. Here, we combine satellite altimeter observations of ice-elevation change and measurements of ice geometry to track grounding-line movement around the entire continent, tripling the coverage of previous surveys. Between 2010 and 2016, 22%, 3%, and 10% of surveyed grounding lines in West Antarctica, East Antarctica, and at the Antarctic Peninsula retreated at rates faster than 25 m/yr – the typical pace since the last glacial maximum – and the continent has lost 1463 km^2 ± 791 km^2 of grounded-ice area. Although by far the fastest rates of retreat occurred in the Amundsen Sea Sector, we show that the Pine Island Glacier grounding line has stabilized - likely as a

consequence of abated ocean forcing. On average, Antarctica's fast-flowing ice streams retreat by 110 meters per meter of ice thinning.

Grounding lines are the junction where marine-based ice sheets become sufficiently buoyant to detach from the sea floor and float[1,2]. Knowledge of this position is critical for quantifying ice discharge[3], as a boundary condition for numerical models of ice flow[4], and as an indicator of the ice sheet's state during periods of advance or retreat[1,5]. In Antarctica, grounding lines are of particular interest because ice-shelf thinning and collapse have driven grounding-line retreat and glacial imbalance around the continent[6–8]. Although Antarctic grounding lines have retreat since the Last Glacial Maximum[9], the pace of retreat at several Antarctic ice streams has been much higher during the satellite era[10–15] and numerical simulations have indicated that this rapid retreat may be followed by centennial-scale collapse of the inland catchment areas.[16,17]

Tracking the position of ice-sheet grounding lines using satellite observations has relied on three general approaches; identifying mismatch between surface elevation and freeboard determined through buoyancy calculations[18], breaks in the surface slope associated with the transition from grounded to floating ice[19], and the contrast between vertical motion of floating and grounded ice due to ocean tides[20]. The latter method is by far the most accurate, because it relies on mapping the hinge line – the limit of tidal flexure at the ice surface which is more readily detectable than the grounding line itself[21]. Although grounding-line migration is usually quantified by repeating the above techniques over time[12], the necessary satellite observations have been infrequently acquired, and so estimates exist at only a handful of locations[12–14]. Here, we extend a method[11,13,22] for detecting grounding line motion from satellite measurements of surface-elevation change and airborne surveys of the ice-sheet geometry to produce the first continental-scale assessment of Antarctic grounding-line migration.

Changes in the mass of the firn and ice column around the grounding line cause horizontal migration of the grounding line as the area, in which the ice is buoyant, grows or shrinks. We convert surface-elevation rates, $\frac{\partial s}{\partial t}$, obtained from CryoSat-2 observations[23] into rates of grounding-line migration, v_{GL}, at known grounding-line locations (see Methods for a detailed derivation):

$$v_{\mathrm{GL}} = \left[-(\alpha + (\rho_{\mathrm{o}}/\rho_{\mathrm{i}} - 1)\beta)^{-1}\right] \frac{\rho_{\mathrm{m}}}{\rho_{\mathrm{i}}} \frac{\partial s}{\partial t}\,.$$

The term in square brackets, which we will refer to as propensity for retreat, takes slopes of the surface (α – also from CryoSat-2) and the bedrock[24] topographies (β) in the direction of grounding-line migration as well as the contrast between ocean (ρ_{o}) and ice densities (ρ_{i}) into account. The material density ρ_{m} allows thickness changes to occur at densities between snow and ice. The direction of grounding-line migration is empirically defined based on grounding-line perpendiculars, flow directions, and bedrock inclinations. We restrict our solution to sections where the grounding-line location has been derived from satellite Interferometric Synthetic Aperture Radar (InSAR)[25] and where the propensity for retreat is not excessively high (Figure 1). To estimate the overall error, we consider uncertainties in the density assumptions, satellite-derived surface elevation and elevation rate, and bedrock topography. Altogether, we are able to quantify grounding-line migration along 33.4% of Antarctica's 47,000 km grounding line, including 61 glacier basins[3] – three times the combined length and four times as many glaciers as mapped in previous surveys.[11–14,19]

We estimate that, between 2010 and 2016, 10.7% of the Antarctic grounding line retreated and 1.9% advanced faster than 25 m/yr, the typical rate of ice-stream retreat during the last deglaciation[26,27]. There were notable regional differences: Whilst the Peninsula matched this overall picture quite well (9.5% retreating, 3.5% advancing), the West Antarctic Ice Sheet saw 21.7% retreating (59.4% in the Amundsen Sea Sector) and only 0.7% advancing, whereas the grounding line of the East Antarctic Ice Sheet retreated and advanced in 3.3% and 2.2% of its length, respectively (Table S1). These changes amounted to a net 209 km^2 ± 113 km^2 loss of grounded-ice area per year over the CryoSat-2 period in the surveyed sections, of which the major part took place along the West Antarctic Ice Sheet (177 km^2 ± 48 km^2).

Large-scale patterns of grounding-line retreat (Figure 1) coincided with sectors in which ice streams are known to be thinning (see Figure S1), for example at the Amundsen and Bellingshausen Sea coasts of West Antarctica[23,28]. This general link is modulated by the local ice-sheet geometry (propensity), which introduces higher spatial variability into the pattern of retreat. Bedrock slopes along swathes of the English Coast and Wilkes Land make these sectors unfavorable for either retreat or advance, despite the relatively large changes in ice-sheet thickness that have occurred. Long sections were in a state of advance in Dronning Maud Land, East Antarctica, where mass gains have been associated with increased snow accumulation[29,30].

To investigate regional patterns of grounding-line migration, we examine changes within 61 drainage basins[3] (Figure 1). Highly localized extremes of rapid grounding-line retreat between 500 m/yr and 1200 m/yr have occurred at Fleming, Thwaites, Haynes, Pope, Smith, Kohler, and Hull Glaciers, at Ferrigno Ice Stream, and at glaciers feeding the Getz Ice Shelf, all draining into either the Amundsen Sea or the Bellingshausen Sea, where broad sections of the coast have retreated at rates of 300 m/yr and 100 m/yr, respectively. In East Antarctica, Frost and Totten Glaciers have retreated, locally, at rates of up to 200 m/yr, whereas Mercer and

Dibble Ice Streams and glaciers of the Budd Coast have advanced, locally, at up to 60 m/yr to 230 m/yr.

In general, fast grounding-line migration occurs in areas of fast ice flow (Figure S2), and so we also computed average rates of migration in areas where the ice speed exceeds 25 m/yr and 800 m/yr (Figure 1, Table S2). In total, the central portions of ten fast flowing ice streams have retreated at rates of more than 50 m/yr on average (applying either of the two thresholds), including those of the Amundsen Sea, Totten Glacier, and several in the Bellingshausen Sea – areas in which change is known to be driven at least partially by warm ocean water[31–34]. The fast flowing sections of Lidke Glacier, Berg Ice Stream, and glaciers flowing into Venable and Abbot Ice Shelves have also retreated, albeit at slower average rates of up to 50 m/yr. Elsewhere in East Antarctica, rates of migration are mostly centered around zero, apart from Frost, Denman and Recovery Glaciers which have retreated at average rates between 19 and 45 m/yr, and from Mertz, Budd, and Shirase Glaciers and Slessor Ice Stream, which advanced at average rates between 14 and 48 m/yr.

Widespread grounding-line retreat has been recorded in the Amundsen Sea Embayment using satellite InSAR[11,12], with which we contrast our altimetry-based results. At Thwaites Glacier, the average rate of grounding-line retreat has increased from 340 ± 280 m/yr between 1996 and 2011[12] to 420 ± 240 m/yr according to our method (Figure 2A). Retreat at Pine Island Glacier appears to have stagnated at 40 m/yr ± 30 m/yr during the CryoSat-2 period, after it migrated inland at a rate of around 1 km/yr between 1992 and 2011 as documented by the previous studies[11] (Figure 2B). The recent stagnation coincides with a deceleration of thinning from 5 m/yr in ~2009 to less than 1 m/yr across a 20 km section inland of the 2011 grounding line[35], which in principle explains the reduced retreat rate. The slowdown in surface lowering could, however, also be due to further ungrounding, and so we first examine this possibility:

To maintain contact with the upstream parts of the ~120 km long central trunk, which are in our data thinning at a maximum rate of 2 m/yr (Figure S3), the grounding line would have had to retreat by at least 15 km since 2011 – more than double that of the previous two decades[11,12], at a time when thinning has abated across the lower reaches of the glacier. This leads us to conclude that the main trunk's grounding line has stabilized, potentially due to the absence of warm sub-shelf water[36] which drove retreat until 2011. This finding is supported by two recent studies[37,38], which also report a substantial reduction in the pace of retreat since 2011.

We also observe a continuation of retreat at other, less frequently sampled ice streams. For example, high local rates of retreat of ~1.2 km/yr in our results on Haynes, Smith and Kohler glaciers are comparable to peak rates of 1.8 to 2.0 km/yr detected by InSAR between 1992 and 2014[12,15]. In the Bellingshausen Sea, slower rates of retreat recorded over the last 40 years[13] are similar to those we have derived; at Ferrigno Ice Stream, rates of retreat remain in the range 50 to 200 m/yr, at Lidke Glacier, Berg Ice Stream, Venable and Abbot Ice Shelves, our rates of retreat are in the range of 10 to 40 m/yr compared to the multi-decadal range of 10 to 90 m/yr[13], and at the Cosgrove Ice Shelf we detect no significant retreat, in agreement with previously observed rates between -40 m/yr and +11 m/yr[13]. In East Antarctica, Totten Glacier is the only location where grounding-line retreat has been documented, and our result of 154 m/yr ± 24 m/yr retreat in its fast-flowing section is consistent with the maximum rate of 176 m/yr recorded between 1996 and 2013[14].

We compared rates of ice thickness change and grounding-line migration to assess the degree to which the processes are related (Figure 3). Within ice-stream sections flowing faster than 800 m/yr, thickness changes and grounding-line migration were approximately proportional with 110 ± 6 metres of retreat occurring with each metre of ice thinning. This comparison for the first time informs on the remarkably consistent geometry-driven propensity for retreat at these ice streams, leading to an intimate relation between thinning and retreat, despite very different processes driving them[30,31,39]. A possible reason for this stable relationship is that the geometry at fast moving ice-sheet margins may be comparable due to the involved processes: The shape of the surface topography is formed by the nonlinear viscous flow of ice and the sliding conditions at the bedrock[40]. In turn, bedrock topography emerges through tectonical evolution and pre-glacial erosion, and is interactively shaped by the ice-dynamical environment via sedimental erosion through overriding and subglacial hydrology[41] and via glacial-isostatic adjustment of the solid Earth to the overlying ice mass[42]. Even though these processes occur on different spatial and temporal scales and depend on many parameters, it appears that the average propensity for retreat can nevertheless be approximated for different geological settings – a convenient proxy relationship that may be used as a benchmark in investigations which cannot rely on detailed glacial geometry or dynamics.

We have compiled the first comprehensive record of present-day rates of grounding-line migration around Antarctica, spanning one third of the continent's margin. In the Amundsen and Bellingshausen Sea sectors of West Antarctica and at Totten Glacier, our results complement and extend earlier assessments of grounding-line retreat[11–14], and elsewhere we provide the first observations of migration in key sectors, such as in the Getz Ice Shelf and large parts of East Antarctica and the Peninsula (Figure 1). Although most of the grounding line is stable, we estimate that 3.3%, 21.7%, and 9.5% of East Antarctica, West Antarctica, and the Antarctic Peninsula, respectively, are measurably in a state of retreat. By far the largest rates of grounding-line retreat (> 50 m/yr) occur at ice streams flowing into the Amundsen and Bellingshausen Sea which, on average, are retreating at rates of 134 m/yr and 57 m/yr, as well as at Totten Glacier, all of which experience glacial change driven by warm ocean water[32,33,43], indicating that the ocean as a driver generates fastest retreat today. The alternation between retreat and advance of glaciers in Wilkes Land could be explained by regional drivers of migration being surpassed by local ones in places. There is a robust relationship between changes in ice thickness and grounding-line migration at Antarctic outlet glaciers, indicating that the geometrical propensity for retreat is relatively uniform in areas of fast flow. The extent of our record could be substantially increased with a more detailed map of the grounding-line position, ideally acquired in the same period as satellite altimetry observations. Overall, our method is a novel and potent approach for detecting and monitoring ice-sheet imbalance in Antarctica; it can be used to pinpoint locations which merit more detailed analysis through field campaigns or dedicated InSAR surveys, e.g. where fast migration occurs or a high geometric propensity for retreat prevails.

References

1. Weertman, J. Stability of the junction of an ice sheet and an ice shelf. J. Glaciol. **13,** 3–11 (1974).
2. Schoof, C. Ice sheet grounding line dynamics: Steady states, stability, and hysteresis. J. Geophys. Res. **112,** F03S28 (2007).
3. Rignot, E. et al. Recent Antarctic ice mass loss from radar interferometry and regional climate modelling. Nat. Geosci. **1,** 106–110 (2008).
4. Docquier, D., Perichon, L. & Pattyn, F. Representing Grounding Line Dynamics in Numerical Ice Sheet Models: Recent Advances and Outlook. Surv. Geophys. **32,** 417–435 (2011).
5. Pollard, D. & DeConto, R. M. Modelling West Antarctic ice sheet growth and collapse through the past five million years. Nature **458,** 329–332 (2009).

6. Scambos, T. A., Bohlander, J. A., Shuman, C. A. & Skvarca, P. Glacier acceleration and thinning after ice shelf collapse in the Larsen B embayment, Antarctica. Geophys. Res. Lett. **31,** L18402 (2004).

7. Shepherd, A. et al. Recent loss of floating ice and the consequent sea level contribution. Geophys. Res. Lett. **37,** L13503 (2010).

8. Rignot, E., Jacobs, S., Mouginot, J. & Scheuchl, B. Ice-Shelf Melting Around Antarctica. Science **341,** 266–270 (2013).

9. Bentley, M. J. et al. A community-based geological reconstruction of Antarctic Ice Sheet deglaciation since the Last Glacial Maximum. Quat. Sci. Rev. **100,** 1–9 (2014).

10. Rignot, E. J. Fast Recession of a West Antarctic Glacier. Science **281,** 549–551 (1998).

11. Park, J. W. et al. Sustained retreat of the Pine Island Glacier. Geophys. Res. Lett. **40,** 2137–2142 (2013).

12. Rignot, E., Mouginot, J., Morlighem, M., Seroussi, H. & Scheuchl, B. Widespread, rapid grounding line retreat of Pine Island, Thwaites, Smith, and Kohler glaciers, West Antarctica, from 1992 to 2011. Geophys. Res. Lett. **41,** 3502–3509 (2014).

13. Christie, F. D. W., Bingham, R. G., Gourmelen, N., Tett, S. F. B. & Muto, A. Four-decade record of pervasive grounding line retreat along the Bellingshausen margin of West Antarctica. Geophys. Res. Lett. **43,** 5741–5749 (2016).

14. Li, X., Rignot, E., Morlighem, M., Mouginot, J. & Scheuchl, B. Grounding line retreat of Totten Glacier, East Antarctica, 1996 to 2013. Geophys. Res. Lett. **42,** 8049–8056 (2015).

15. Scheuchl, B., Mouginot, J., Rignot, E., Morlighem, M. & Khazendar, A. Grounding line retreat of Pope, Smith, and Kohler Glaciers, West Antarctica, measured with

Sentinel-1a radar interferometry data. Geophys. Res. Lett. **43,** 8572–8579 (2016).

16. Joughin, I., Smith, B. E. & Medley, B. Marine Ice Sheet Collapse Potentially Under Way for the Thwaites Glacier Basin, West Antarctica. Science **344,** 735–738 (2014).

17. DeConto, R. M. & Pollard, D. Contribution of Antarctica to past and future sea-level rise. Nature **531,** 591–597 (2016).

18. Fricker, H. A. et al. Redefinition of the Amery Ice Shelf, East Antarctica, grounding zone. J. Geophys. Res. Solid Earth **107,** ECV 1-1-ECV 1-9 (2002).

19. Horgan, H. J. & Anandakrishnan, S. Static grounding lines and dynamic ice streams: Evidence from the Siple Coast, West Antarctica. Geophys. Res. Lett. **33,** 1–6 (2006).

20. Goldstein, R. M., Engelhardt, H., Kamb, B. & Frolich, R. M. Satellite Radar Interferometry for Monitoring Ice Sheet Motion: Application to an Antarctic Ice Stream. Science **262,** 1525–1530 (1993).

21. Gray, L. et al. RADARSAT interferometry for Antarctic grounding-zone mapping. Ann. Glaciol. **34,** 269–276 (2002).

22. Shepherd, A., Wingham, D. J. & Mansley, J. A. D. Inland thinning of the Amundsen Sea sector, West Antarctica. Geophys. Res. Lett. **29,** 2–4 (2002).

23. McMillan, M. et al. Increased ice losses from Antarctica detected by CryoSat-2. Geophys. Res. Lett. **41,** 3899–3905 (2014).

24. Fretwell, P. et al. Bedmap2: improved ice bed, surface and thickness datasets for Antarctica. Cryosph. **7,** 375–393 (2013).

25. Rignot, E., Mouginot, J. & Scheuchl, B. Antarctic grounding line mapping from differential satellite radar interferometry. Geophys. Res. Lett. **38,** L10504 (2011).

26. Smith, J. A. et al. New constraints on the timing of West Antarctic Ice Sheet retreat in

the eastern Amundsen Sea since the Last Glacial Maximum. Glob. Planet. Change **122,** 224–237 (2014).

27. Pollard, D., Chang, W., Haran, M., Applegate, P. & DeConto, R. Large ensemble modeling of the last deglacial retreat of the West Antarctic Ice Sheet: comparison of simple and advanced statistical techniques. Geosci. Model Dev. **9,** 1697–1723 (2016).

28. Pritchard, H. D., Arthern, R. J., Vaughan, D. G. & Edwards, L. A. Extensive dynamic thinning on the margins of the Greenland and Antarctic ice sheets. Nature **461,** 971–975 (2009).

29. Lenaerts, J. T. M. et al. Recent snowfall anomalies in Dronning Maud Land, East Antarctica, in a historical and future climate perspective. Geophys. Res. Lett. **40,** 2684–2688 (2013).

30. Boening, C., Lebsock, M., Landerer, F. & Stephens, G. Snowfall-driven mass change on the East Antarctic ice sheet. Geophys. Res. Lett. **39,** L21501 (2012).

31. Jenkins A. et al. Observations beneath Pine Island Glacier in West Antarctica and implications for its retreat. Nat. Geosci. **3,** 468–472 (2010).

32. Rintoul, S. R. et al. Ocean heat drives rapid basal melt of the Totten Ice Shelf. Sci. Adv. **2,** e1601610 (2016).

33. Holland, P. R., Jenkins, A. & Holland, D. M. Ice and ocean processes in the Bellingshausen Sea, Antarctica. J. Geophys. Res. Ocean. **115,** C05020 (2010).

34. Hogg, A. E. et al. Increased ice flow in Western Palmer Land linked to ocean melting. Geophys. Res. Lett. **44,** 4159–4167 (2017).

35. Konrad, H. et al. Uneven onset and pace of ice-dynamical imbalance in the Amundsen Sea Embayment, West Antarctica. Geophys. Res. Lett. **44,** 910–918 (2017).

36. Dutrieux, P. et al. Strong Sensitivity of Pine Island Ice-Shelf Melting to Climatic Variability. Science **343,** 174–178 (2014).

37. Joughin, I., Shean, D. E., Smith, B. E. & Dutrieux, P. Grounding line variability and subglacial lake drainage on Pine Island Glacier, Antarctica. Geophys. Res. Lett. **43,** 9093–9102 (2016).

38. Milillo, P. et al. On the Short-term Grounding Zone Dynamics of Pine Island Glacier, West Antarctica, Observed With COSMO-SkyMed Interferometric Data. Geophys. Res. Lett. **44,** 436-444 (2017).

39. Joughin, I. et al. Continued deceleration of Whillans ice stream West Antartica. Geophys. Res. Lett. **32,** L22501 (2005).

40. Robin, G. de Q. Surface Topography of Ice Sheets. Nature **215,** 1029–1032 (1967).

41. Smith, A. M. et al. Rapid erosion, drumlin formation, and changing hydrology beneath an Antarctic ice stream. Geology **35,** 127–130 (2007).

42. van den Berg, J., van de Wal, R. S. W., Milne, G. A. & Oerlemans, J. Effect of isostasy on dynamical ice sheet modeling: A case study for Eurasia. J. Geophys. Res. **113,** B05412 (2008).

43. Jacobs, S. S., Jenkins, A., Giulivi, C. F. & Dutrieux, P. Stronger ocean circulation and increased melting under Pine Island Glacier ice shelf. Nat. Geosci. **4,** 519–523 (2011).

44. Wessel, P. & Smith, W. H. F. Free software helps map and display data. Eos Trans. AGU **72,** 441 (1991).

45. Mouginot, J., Scheuchl, B. & Rignot, E. Mapping of Ice Motion in Antarctica Using Synthetic-Aperture Radar Data. Remote Sens. **4,** 2753–2767 (2012).

Acknowledgements

We acknowledge the European Space Agency (ESA) for the provision of CryoSat-2 data and ESA's Antarctic_Ice Sheet_cci as well as the UK Natural Environment Research Council's (NERC) Centre for Polar Observation and Modelling (CPOM) for processing of these data. HK. was funded through the NERC's iSTAR Programme and NERC Grant Number NE/J005681/1. AEH was supported by an independent research fellowship (no. 4000112797/15/I-SBo) jointly funded by ESA, the University of Leeds, and the British Antarctic Survey. The figures were produced using the Generic Mapping Tool[44].

Author contributions

HK, AS, AEH, and MM designed the study. LG and AM processed CryoSat-2 data. HK, AS, AEH, MM, and TS analyzed the results. HK and AS wrote the manuscript. All authors contributed to revising the manuscript.

Corresponding author

Hannes Konrad, hannes.konrad@awi.de

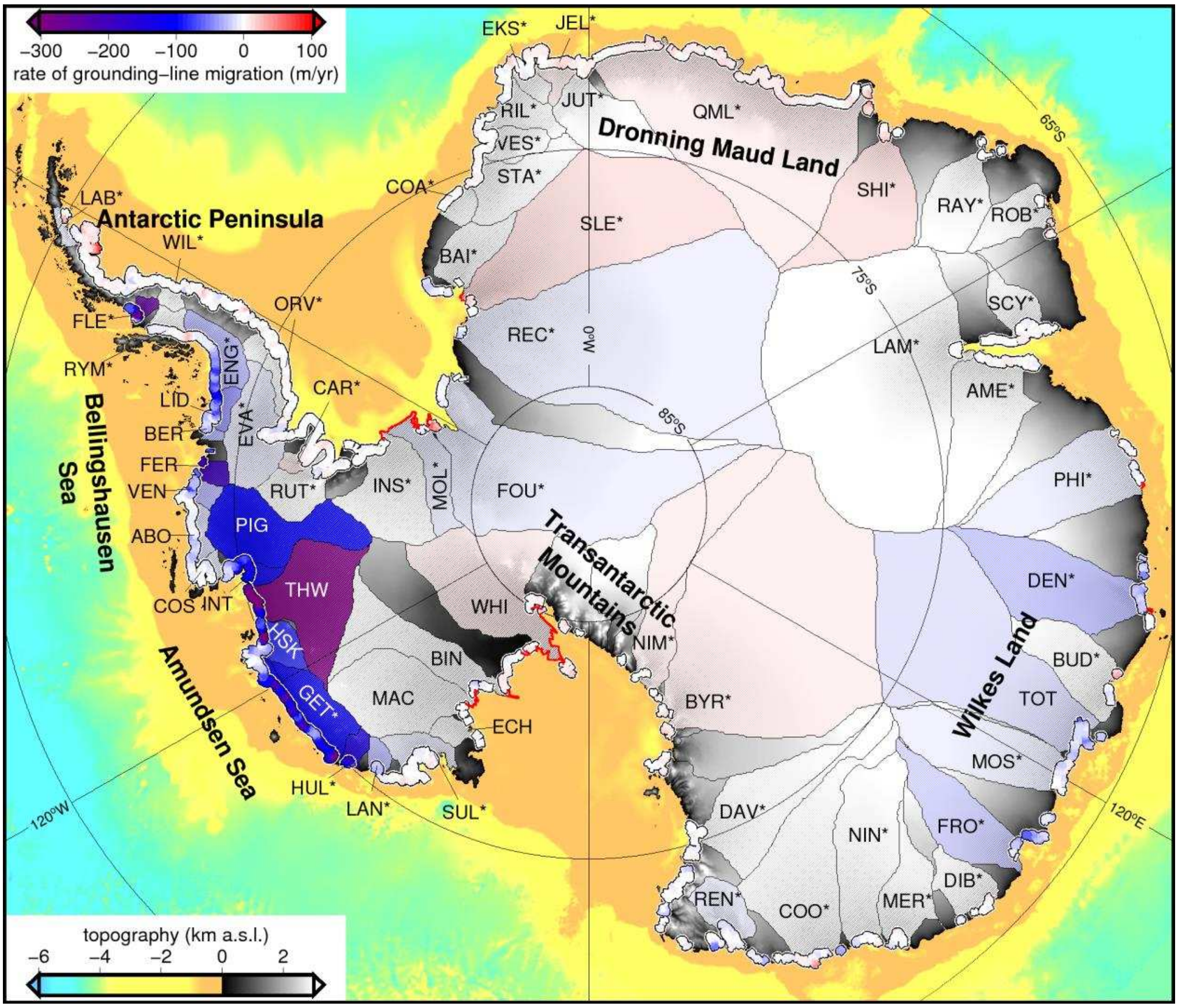

Caption Figure 1

Rates of grounding-line migration between 2010 and 2016 along the Antarctic grounding line[8] derived from CryoSat-2 and bedrock topography[24] observations. Red lines indicate long (>30 km) sections of high propensity for retreat (>500), which we excluded from our analysis. Color-coded basins[3] illustrate rates averaged in the areas flowing faster than 25 m/yr (see also Table S2); basins for which we provide the first estimate of grounding-line retreat during the satellite era are marked with an asterisk. Background colors indicate the bathymetry in the ice shelves and ocean and the ice sheet's surface elevation[24].

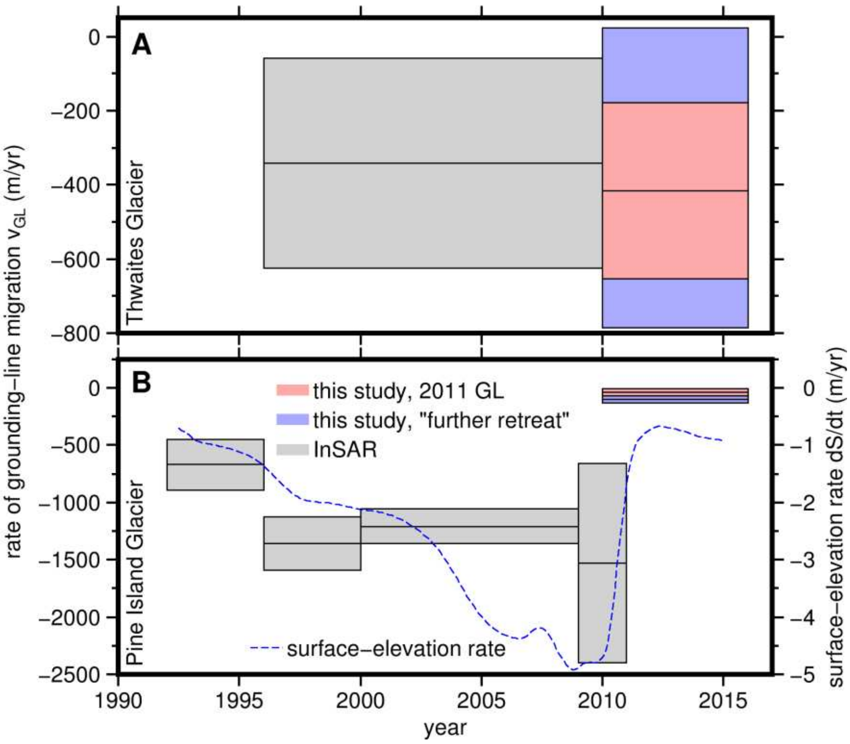

Caption Figure 2

Continuation of rates of grounding-line migration in the Amundsen Sea[11,12] by our approach. Rates are averaged across a 43 km wide along-flow swath defined using velocity observations[45] at Thwaites Glacier (A) and across the central 10 km of Pine Island Glacier (B), evaluated along the 2011 grounding line and in a 'further retreat' scenario designed to investigate the impact of strongly dislocated grounding lines (see Methods). Uncertainties comprise the average local uncertainties in the respective sections and the rates' spatial variabilities therein. Also shown in B is a long-term time series of surface-elevation rates upstream of the 2011 grounding line[35].

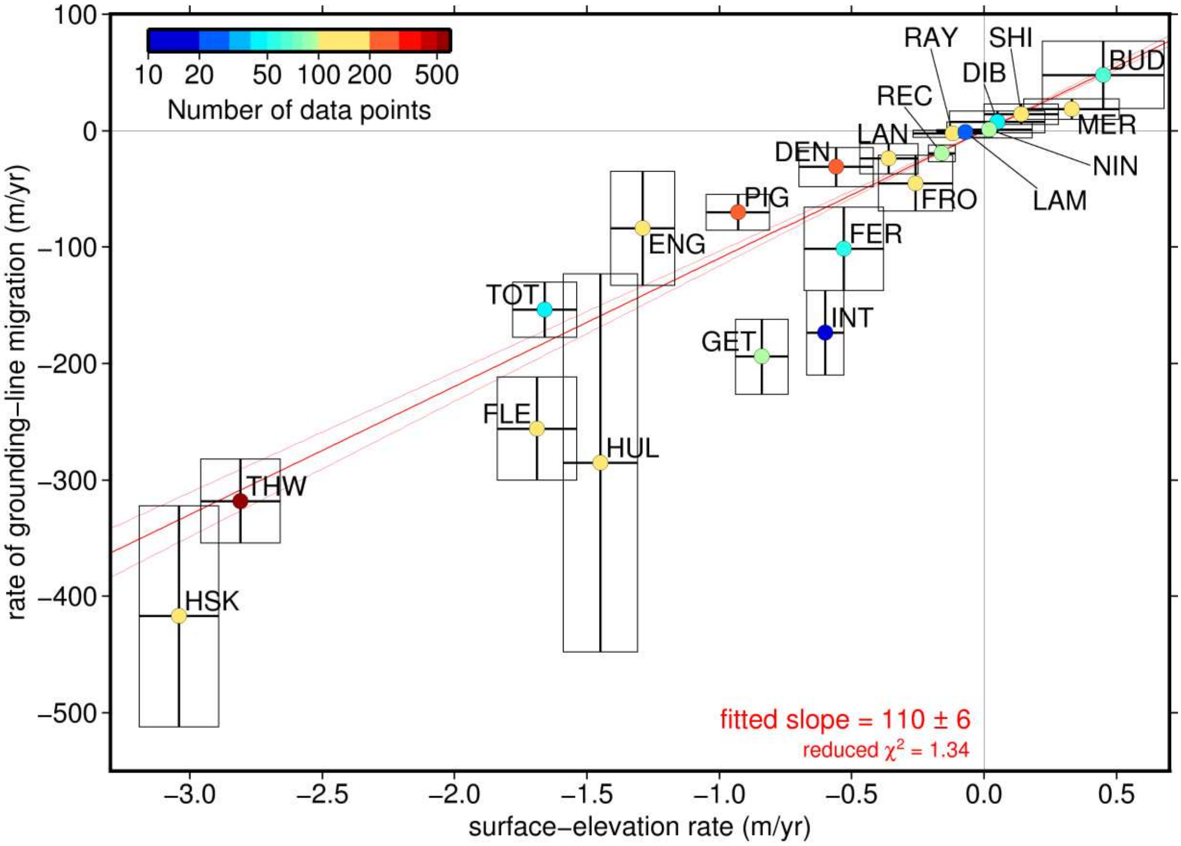

Caption Figure 3

Rates of grounding-line migration versus rates of surface elevation. Both are averaged over fast (>800 m/yr) flowing sections of 21 Antarctic drainage basins. Uncertainties comprise the average local uncertainties of the rates in the respective sections and the spatial variabilities in these sections. Also shown is a straight line fitted in a total least squares sense to these data after re-weighting the average uncertainties by the square root of the number of data points (color coded) in each basin.

Methods

We base our analysis of grounding-line migration on a hydrostatic consideration: While the mass (per unit area) of the ice column σ_i is smaller than that of the water column σ_o in the ice shelves and vice versa for a (marine-based) ice sheet, they are equal directly at the grounding line:

$$[\sigma_\mathrm{i} - \sigma_\mathrm{o}]_\mathrm{GL} = 0 \, . \qquad \text{Eq. (1)}$$

At the grounding line and in the interior of an ice sheet, the mass of the ice column can be expressed in terms of the average density of snow, firn, and ice in the column, ρ_i, the ice sheet's surface elevation, S, and the bedrock topography, B:

$$\sigma_\mathrm{i} = \rho_\mathrm{i}(S - B) \, . \qquad \text{Eq. (2)}$$

Likewise, σ_o can be similarly expressed where the bedrock topography lies below sea level, substituting S by sea-level height E:

$$\sigma_\mathrm{o} = \rho_\mathrm{o}(E - B) \, . \qquad \text{Eq. (3)}$$

Here, ρ_o is the vertically averaged density in the ocean water column. As S and B are usually referenced to E, we assume $E \equiv 0$.

The total temporal derivative of the left-hand side in Eq. (1) containing both partial derivatives and advective contributions related to grounding-line motion by horizontal velocity $\vec{v}_\mathrm{GL}$ must also equal zero.

$$\left[\frac{\partial \sigma_\mathrm{i}}{\partial t} + \vec{v}_\mathrm{GL} \cdot \vec{\nabla}\sigma_\mathrm{i} - \frac{\partial \sigma_\mathrm{o}}{\partial t} - \vec{v}_\mathrm{GL} \cdot \vec{\nabla}\sigma_\mathrm{o}\right]_\mathrm{GL} = 0 \, . \qquad \text{Eq. (4)}$$

Eq. (2) and (3) allow us to replace σ_o and σ_i by the densities and geometric quantities. However, the term $\frac{\partial \sigma_\mathrm{i}}{\partial t}$ needs special consideration: If neglecting basal melt, ice thickness changes are consequences of surface processes (surface mass balance, i.e. interaction with the atmosphere; contribution $\dot{h}_{\mathrm{surf}}$), of firn compaction (contribution $\dot{h}_{\mathrm{fc}}$), and of ice dynamics (contribution $\dot{h}_{\mathrm{ice}}$)[46]:

$$\frac{\partial(S-B)}{\partial t}=\dot{h}_{\mathrm{surf}}+\dot{h}_{\mathrm{fc}}+\dot{h}_{\mathrm{ice}}\ . \qquad \text{Eq. (5)}$$

These contribute differently to the mass σ_{i}: Ice-dynamical thinning or thickening $\dot{h}_{\mathrm{ice}}$ would change the mass at ρ_{i}, snow fall variations $\dot{h}_{\mathrm{surf}}$ would change it at lower densities, firn compaction does not affect the mass at all.[47] We thus introduce the ad hoc 'material density', ρ_{m} to represent which of the above processes is dominant (e.g. McMillan et al.[23]):

$$\frac{\partial\sigma_{\mathrm{i}}}{\partial t}=\rho_{\mathrm{m}}\frac{\partial(S-B)}{\partial t}\ . \qquad \text{Eq. (6)}$$

The introduction of this material density allows us to rearrange Eq. (4):

$$\left[f_1\frac{\partial S}{\partial t}+\vec{v}_{\mathrm{GL}}\cdot\vec{\nabla}(S+f_2B)\right]_{\mathrm{GL}}=0. \qquad \text{Eq. (7)}$$

Here, it is $f_1=\rho_{\mathrm{m}}/\rho_{\mathrm{i}}$ and $f_2=\rho_{\mathrm{o}}/\rho_{\mathrm{i}}-1\approx 0.15$. We have neglected any contributions from bedrock motion (including sea-level rise or similar), as $\frac{\partial B}{\partial t}$ is assumed to contribute ~1 cm/yr at maximum only, if we assume it to be governed by viscoelastic bedrock motion due to paleo ice-mass changes[48].

Assuming that we know the direction of grounding-line motion $\vec{n}$ (i.e. $\vec{v}_{\mathrm{GL}}=v_{\mathrm{GL}}\,\vec{n}$), we define the propensity for retreat as $P=-\left[\vec{n}\cdot\vec{\nabla}(S+f_2B)\right]^{-1}$ (high absolute values indicate a geometry that favors migration; low values occur in stable areas) and solve for the magnitude of the rates of grounding-line migration:

$$v_{\mathrm{GL}}=\left[f_1P\frac{\partial S}{\partial t}\right]_{\mathrm{GL}}=-\left[\frac{\rho_{\mathrm{m}}}{\rho_{\mathrm{i}}}\left(\vec{n}\cdot\vec{\nabla}\left(S+\left[\frac{\rho_{\mathrm{o}}}{\rho_{\mathrm{i}}}-1\right]B\right)\right)^{-1}\frac{\partial S}{\partial t}\right]_{\mathrm{GL}}\ . \qquad \text{Eq. (8)}$$

We obtain S and $\frac{\partial S}{\partial t}$ from CryoSat-2[23] and B from Bedmap2[24] and make reasonable assumptions for densities. The two critical points in our approach are the direction of motion $\vec{n}$ and where to evaluate the respective fields. The uncertainty in $\vec{v}_{\mathrm{GL}}$ is calculated from the individual uncertainties associated with the altimetry measurements[23], Bedmap2 bedrock topography[24], and density assumptions and ranges from 4 cm/yr to 2.5 km/yr, with 90% of all data points between 40 cm/yr and 23 m/yr. Surface-elevation rates and the propensity for retreat along the grounding line are shown in Figure S1.

Surface elevation and surface-elevation rates from CryoSat-2

Surface-elevation measurements by CryoSat-2 in SARIn mode between 2010 and 2016 were binned into 5 km x 5 km grid cells. A function quadratic in the component-wise differences x and y to the cell's centre in polar stereographic coordinates and linear in time t since the centre of the time interval for which observations are available is fitted to the data in each cell in a least-squares sense[23,35],

$$f(x, y, t) = a_0 + a_1 x + a_2 y + a_3 xy + a_4 x^2 + a_5 y^2 + a_6(h) + bt. \qquad \text{Eq. (9)}$$

The offset between ascending and descending track (heading h) was corrected for by fitting respective parameters $a_6(h)$.[49] The parameter $a_0 \equiv S$ represents the grid cell's mean surface elevation as used in P in Eq. (8), and the parameter $b \equiv \frac{\partial S}{\partial t}$ is the respective change rate. The uncertainty of the retrieved surface elevation is given by the root mean square of the differences between residues in each grid cell. The uncertainty of the change rates is given through the one-sigma confidence interval of the respective fit parameter. The data were smoothed by a median filter with a 3 cell-wide window (separately for floating and grounded ice in the case of the rates) before they are interpolated (bilinearly for surface elevation and nearest neighbor for surface-elevation rates) onto the 1 km x 1 km Bedmap2 grid (see below).

After regridding, the surface gradient was determined, which was again smoothed by a median filter with a 5 cell-wide window. This smoothing as well as that of the bedrock gradients (see below) approximately accounted for the grounding line experiencing different rates solely through the presence of a different geometry as it moved.

Bedrock topography from Bedmap2

The bedrock topography B in P in Eq. (8) and its uncertainty between 66 m and 1008 m (not necessarily peaking at the grounding line) were taken from the Bedmap2 data set[24] available on a 1 km x 1 km grid. Gradients of bedrock topography were computed and the respective components were smoothed by applying a 5 cell-wide median filter.

Density assumptions

The ocean water density was assumed to be $\rho_\mathrm{o} = 1027\,\frac{\mathrm{kg}}{\mathrm{m}^3} \pm 5\,\frac{\mathrm{kg}}{\mathrm{m}^3}$.[50] Mean ice density in the column was considered to be $\rho_\mathrm{i} = 887\,\frac{\mathrm{kg}}{\mathrm{m}^3} \pm 23\,\frac{\mathrm{kg}}{\mathrm{m}^3}$, allowing for only ice being present or an approximately 100 m thick firn layer on top of the ice at an average thickness of 1000 m at the two extremes of this choice. There are no Antarctic-wide observations available that show how much of a thickness change in a certain area is due to ice-dynamical imbalance or due to (interannual, decadal, or centennial) trends in snow fall; in the absence of such information, we opted for an empirical scheme to define the material density and mostly utilized the surface-elevation rates as a guidance: An absolute rate below 0.3 m/yr was defined to stem from snow fall anomalies only, $\rho_\mathrm{m} = 400\,\frac{\mathrm{kg}}{\mathrm{m}^3} \pm 50\,\frac{\mathrm{kg}}{\mathrm{m}^3}$. Even if this assumption proved dubious in places, it affected our results only lightly as respective low surface-elevation rates mostly did not translate to large rates of grounding-line migration. An absolute surface-elevation rate above 1 m/yr, as well as all the area along the Amundsen Sea Embayment and Getz Ice Shelf, was assumed to stem from ice-dynamical imbalance mainly, so that we set $\rho_{\mathrm{m}} = 850\,\frac{\mathrm{kg}}{\mathrm{m}^3} \pm 50\,\frac{\mathrm{kg}}{\mathrm{m}^3}$. Anywhere else, we acknowledged that both processes could happen at a similar extent by defining $\rho_{\mathrm{m}} = 625\,\frac{\mathrm{kg}}{\mathrm{m}^3} \pm 175\,\frac{\mathrm{kg}}{\mathrm{m}^3}$. Such a superposition has, for example, been observed along the English Coast where both ice-dynamical imbalance and decreasing snow fall lead to thinning[34]. The density uncertainties also accommodate the error arising from assuming a hydrostatic equilibrium at the grounding line where in fact elastic flexure of the stiff ice body leads to a local deviation from this equilibrium.

Direction of grounding-line motion

We had to make a relatively strong assumption about the direction of grounding-line motion $\vec{n}$ because there is only one equation for the two-component vector $\vec{v}_{\mathrm{GL}}$. Here, we implemented three different assumptions:

1. The grounding line advanced in direction of ice flow (positive values of v_{GL}) and retreated in opposite direction (negative values). The same assumption has implicitly been made in other studies by evaluating grounding-line retreat along flow[11–13]. Flow directions were obtained by bilinearly interpolating surface velocities[45] to the grounding-line coordinates.
2. The grounding line advanced (positive) and retreated (negative) perpendicular to the grounding line (represented by the normal vector $\vec{n}_{\mathrm{GL}}$ obtained from finite differences of the grounding-line coordinates).
3. Where the bedrock gradient points seawards from the grounding line ($\vec{n}_{\mathrm{GL}} \cdot \vec{\nabla} B > 0$), the grounding line was assumed to advance (positive) in the direction of this gradient or retreat (negative) in the opposite direction. By that, grounding lines would have

migrated towards shallower ocean bathymetry or retreated towards deeper bathymetry. This would be in accordance with the so-called Marine Ice Sheet Instability hypothesis[2], which considers grounding lines on retrograde slopes inherently unstable in the absence of lateral stresses. Where the bedrock gradient points inwards, a similar argument would not have held anymore, which is why we then opted for the normal vector $\vec{n}_{\mathrm{GL}}$ as in option 2.

We note that the results from any two of the three options agree within errors for 88.4% of the considered grounding-line sections between options 1 and 3, and for 98.3% between options 2 and 3. We consider option 3 to have the strongest physical basis and thus present mainly these data. The only exception is the 'further retreat' scenario on Pine Island and Thwaites Glaciers (see below) for which, in the absence of an actual grounding-line position and thus normal vectors upstream of the 2011 position, we chose option 1 as it supplied us with a continuous field of directional vectors.

Grounding-line locations and data editing

We evaluated all respective fields (available on the Bedmap2 1 km x 1 km grid, see above) along the grounding line[8] where it was determined from InSAR, i.e. where the respective sections are also present in the MEaSUREs data set[25] (46% of the total grounding line), using bilinear interpolation and then solved for the rate of grounding-line migration (Eq. (8)). We note that the grounding-line positions in fast changing areas like the Amundsen Sea Embayment were also among the most recently updated (observations from 2011). At some locations, the last observations were from the 1990s. As no other region showed an equal extent of imbalance as the Amundsen Sea Embayment, we consider respective observations to be sufficiently up-to-date for a well-informed result from our approach.

Our assumption of a hydrostatic equilibrium only makes sense where the ice flows into an ice shelf rather than forming grounded ice cliffs; therefore, we rejected data points which do not separate grounded and floating ice as identified using the respective ice sheet/ice shelf/ocean mask in the Bedmap2 data set (29% of all data points) or at which the Bedmap2 bedrock topography is above sea level (12%). Areas which proved to be highly sensitive to surface-elevation change (absolute propensity above 500) were also discarded (15%, Figure 1, and Figure S1. This latter condition excludes, for example, sections of the Siple Coast and Möller and Institute Ice Streams flowing into the Ronne-Filchner Ice Shelf which, though stagnant today, are very lightly grounded[19] and may therefore merit dedicated InSAR monitoring. It is possible that a better resolved glacier geometry could improve the results in these areas. Because we required grounding-line retreat to be caused by thinning and advance to be caused by thickening, we also discarded data points at which $\frac{\partial s}{\partial t}$ and the resulting v_{GL} have a negative relation (i.e. negative propensity) caused by local errors in the assumption of migration direction or the input data (22%). Additional gaps occur where CryoSat-2 does not sample the surface elevation and respective changes (9%). In summary, we discard the solution in about two thirds of the Antarctic margin, manifesting in data gaps which are 12 km wide on average, with 95% of them below 185 km.

Determining portions in retreat and in advance

In order to determine the advancing (retreating) fraction of each region (East Antarctic Ice Sheet, Antarctic Peninsula, West Antarctic Ice Sheet, and – as subsets of the latter – West Antarctica's sectors along the coasts of the Weddell Sea, Ross Sea, Amundsen Sea, Bellingshausen Sea), we summed up the number of points at which we had retained a solution for the rate of grounding-line migration, which were above (below) +25 m/yr (-25 m/yr), and at which the associated uncertainty did not exceed the actual rate. The threshold of 25 m/yr was introduced ad hoc based on modelled and geologically derived retreat rates of a West Antarctic paleo ice stream system[26,27] so that the impact of small rates on these numbers was limited. Detailed numbers are provided in Table S1.

Coincidence of grounding-line migration and fast flow

We evaluated how fast grounding-line migration and fast ice flow are spatially related: The histogram in Figure S2 shows how slow-flowing regions as given by MEaSUREs ice velocities[45] saw less grounding-line migration, and how faster flowing regions were more often experiencing grounding-line migration, also at higher rates. It is also obvious that grounding-line advance was minor compared to retreat.

Glacier identification and glacier-wide averages

In order to be able to discuss rates of grounding-line migration averaged on glaciologically meaningful regional scales, we used 65 glacial entities[3] and extended them to the recent grounding line by adding area downstream of their defined area using MEaSUREs surface velocities[45]. Both the rates of surface elevation and grounding-line migration were averaged for each of these basins in areas where surface velocities[45] exceed 25 m/yr and 800 m/yr respectively (Table S2). Additionally, we report respective average uncertainties and – as a measure for extreme values – the 5- and 95-percentiles within these velocity classes. Depending on the magnitude of surface velocities and availability of rates of grounding-line migration according to the above description, some of the 65 glacier basins are not represented by an average value (e.g. Kamb Ice Stream between Whillans (WHI) and Bindschadler (BIN) Ice Streams), leaving us with 61 basins which actually contain results.

Comparison with InSAR-derived rates at Pine Island and Thwaites Glaciers (Figure 2) and consideration of 'further retreat'

Published results of grounding-line retreat at Pine Island Glacier (1992–2011) are given as the average along a central section and the standard deviation across that section by Park et al[11].To allow comparison, we computed the same quantities for a previously defined cross section on Thwaites glacier from the MEaSUREs grounding-line locations from 1996 and 2011[12,25].

We also consider a 'further retreat' scenario, which is designed to account for potential inland migration of the grounding line since 2011 and thus to provide an upper bound on retreat rates since 2011. It should be noted, however, that a recent survey confirmed that substantial further retreat has not occurred.[38] The 'further retreat' scenario is designed as follows: The coordinates of the 2011 grounding-line observation are advected upstream over the time from its acquisition (2011) to the end of our observational period (2016); the direction is chosen to be opposite of the flow direction according to the MEaSUREs velocity observations; the magnitude of advection speed is chosen to be 1500 m/yr as this roughly equals the maximum rates obtained from the InSAR analysis in the Amundsen Sea Embayment[11,12]. Finally, the average rate of grounding-line retreat in the 'further retreat' scenario was determined using all Bedmap2 grid cells that lie in the area between the 2011 and the inland advected grounding lines, as well as in the respective cross sections on Pine Island and Thwaites glaciers. Here, it was necessary to choose option 1) for the assumed direction of grounding-line motion, i.e. the direction of the flow velocity (see above). The 'further retreat' scenario allows us to assess the maximum impact that an inaccurate grounding-line position (e.g. due to considerable but unmapped retreat since 2011) has on our results.

Our estimated uncertainties of the average altimetry-derived retreat rates along these cross sections (at the 2011 grounding line and upstream of it in the 'further retreat' scenario) include both the standard deviation and the average propagated uncertainties of the single locations.

An overview over the grounding-line situation and the ‘further retreat’ scenario at Thwaites Glacier and Pine Island Glacier can be found in supplementary Figure S3.

Fitted empirical relationship between rates of surface elevation and grounding-line migration (Figure 3)

We investigated the general relationship between rates of surface elevation and grounding-line migration by focusing on the glacier-wide averages from applying the 800 m/yr threshold on ice flow. The empirical relationship of 110 metres of migration for each metre of thickness change was obtained from a linear total-least-squares fit[51] to these data forced through the origin, for which the average uncertainties had been re-weighted according to the square root of the number of data points going into the averaging of the rates, i.e. the width of the surveyed section, in each basin, divided by their overall mean. The surface-elevation rates were not corrected for vertical displacement of the Earth’s surface due to GIA, see above. However, with present-day rates usually estimated to be below 1 cm/yr[48], we expect them to have only a minor impact on our analysis and neglected them here.

Data availability statement

The rates of grounding-line migration results that support the findings of this study are available from the CPOM data portal, http://www.cpom.ucl.ac.uk/csopr/. We acknowledge the authors of all the data sets which we used in this study and which are freely available online. These are the Bedmap2 bedrock topography[24], the MEaSUREs Antarctic velocity map[45,52] and the MEaSUREs Antarctic grounding-line locations[25,53].

References in Methods section

46. Ligtenberg, S. R. M., Horwath, M., van den Broeke, M. R. & Legrésy, B. Quantifying the seasonal ‘breathing’ of the Antarctic ice sheet. Geophys. Res. Lett. **39,** L23501 (2012).

47. Shepherd, A. et al. A Reconciled Estimate of Ice-Sheet Mass Balance. Science **338,** 1183–1189 (2012).

48. Martín-Español, A. et al. An assessment of forward and inverse GIA solutions for Antarctica. J. Geophys. Res. Solid Earth **121,** 6947–6965 (2016).

49. Armitage, T. W. K., Wingham, D. J. & Ridout, A. L. Meteorological Origin of the Static Crossover Pattern Present in Low-Resolution-Mode CryoSat-2 Data Over Central Antarctica. IEEE Geosci. Remote Sens. Lett. **11,** 1295–1299 (2014).

50. Griggs, J. A. & Bamber, J. L. Antarctic ice-shelf thickness from satellite radar altimetry. J. Glaciol. **57,** 485–498 (2011).

51. Krystek, Michael and Anton, M. A least-squares algorithm for fitting data points with mutually correlated coordinates to a straight line. Meas. Sci. Technol. **18,** 3438–3442 (2007).

52. Rignot, E., Mouginot, J. & Scheuchl, B. MEaSUREs InSAR-Based Antarctica Ice Velocity Map. (2011). doi:http://doi.org/10.5067/MEASURES/CRYOSPHERE/nsidc-0484.001

53. Rignot, E., Mouginot, J. & Scheuchl, B. MEaSUREs Antarctic Grounding Line from

Differential Satellite Radar Interferometry, Version 2. Boulder, Color. USA. NASA Natl. Snow Ice Data Cent. Distrib. Act. Arch. Cent. (2016). doi:http://doi.org/10.5067/IKBWW4RYHF1Q